AGU PUBLICATIONS

Geophysical Research Letters

RESEARCH LETTER
10.1002/2015GL065457

Key Points:
- The Paul-Mohr-Coulomb failure criterion includes three principal stresses
- Triaxial compression and extension tests provide data to determine two friction angles
- With true triaxial data, 6- and 12-sided pyramids are constructed with best fit planes

Correspondence to:
R. Y. Makhnenko,
roman.makhnenko@epfl.ch

Citation:
Makhnenko, R. Y., J. Harvieux, and J. F. Labuz (2015), Paul-Mohr-Coulomb failure surface of rock in the brittle regime, *Geophys. Res. Lett.*, *42*, 6975–6981, doi:10.1002/2015GL065457.

Received 20 JUL 2015
Accepted 11 AUG 2015
Accepted article online 14 AUG 2015
Published online 3 SEP 2015

Paul-Mohr-Coulomb failure surface of rock in the brittle regime

Roman Y. Makhnenko[1,2], Justice Harvieux[1], and Joseph F. Labuz[1]

[1]Department of Civil, Environmental, and Geo-Engineering, University of Minnesota, Twin Cities, Minneapolis, Minnesota, USA, [2]Soil Mechanics Laboratory-Chair "Gaz Naturel" Petrosvibri, School of Architecture, Civil and Environmental Engineering, Swiss Federal Institute of Technology, Lausanne, Switzerland

Abstract The Paul-Mohr-Coulomb failure criterion includes the intermediate principal stress σ_{II} and friction angles at the limiting stress states of $\sigma_{II}=\sigma_{III}$ and $\sigma_{II}=\sigma_{I}$, where σ_{I} and σ_{III} are major and minor principal stresses. Conventional triaxial compression ($\sigma_{II}=\sigma_{III}$), extension ($\sigma_{II}=\sigma_{I}$), and plane strain ($\sigma_{I}\neq\sigma_{II}\neq\sigma_{III}$) experiments were performed on dry rock. The failure data were plotted in principal stress space, and material parameters were determined in the context of two internal friction angles and the theoretical uniform triaxial (all-around equal) tensile strength. Assuming isotropy, the triaxial compression and extension results were used to construct a six-sided pyramidal failure surface, and the extension friction angle was larger than the compression friction angle, a sufficient but not necessary condition of the intermediate stress effect. To capture the behavior of the rock in multiaxial loading, the Paul-Mohr-Coulomb criterion was extended to form a 12-sided pyramid with best fit planes.

1. Introduction

To describe failure of rock in the brittle regime, the Mohr-Coulomb (MC) criterion is most popular due to recognizable material parameters (e.g., friction angle and cohesion) and its mathematical simplicity:

$$A\sigma_{I}+C\sigma_{III}=1 \tag{1}$$

where σ_{I} and σ_{III} are major and minor principal stresses and A and C are constants. MC can be written as

$$\frac{\sigma_{I}}{V_o}\left[\frac{1-\sin\phi}{2\sin\phi}\right]-\frac{\sigma_{III}}{V_o}\left[\frac{1+\sin\phi}{2\sin\phi}\right]=1 \tag{2}$$

where φ is the friction angle and V_o is the theoretical uniform triaxial tensile strength, with $V_o\sin\varphi=S_o\cos\varphi$; S_o is the shear stress intercept on a Mohr plane also known as cohesion. Of course, MC is a first-order model of the observed failure response, which exhibits a nonlinear variation of σ_{I} with σ_{III} and, possibly, an effect of the intermediate principal stress σ_{II} [e.g., *Paterson and Wong*, 2005; *Mogi*, 2007; *Haimson and Rudnicki*, 2010; *Ingraham et al.*, 2013; *Cornet*, 2015]. In addition, a tension cutoff is needed when one or more of the principal stresses are tensile, because the uniaxial tensile strength of rock is much less than that predicted from MC [*Paul*, 1961], and porous rock exhibits a "cap" in the failure surface [*Di Maggio and Sandler*, 1971], and this behavior is not represented.

As suggested by *Paul* [1968] and to some extent also by *Haythornthwaite* [1962], equation (1) can be easily modified to include σ_{II}:

$$A\sigma_{I}+B\sigma_{II}+C\sigma_{III}=1 \tag{3}$$

and *Meyer and Labuz* [2013] named this failure criterion Paul-Mohr-Coulomb (PMC):

$$\frac{\sigma_{I}}{V_o}\left[\frac{1-\sin\phi_c}{2\sin\phi_c}\right]+\frac{\sigma_{II}}{V_o}\left[\frac{\sin\phi_c-\sin\phi_e}{2\sin\phi_c\sin\phi_e}\right]-\frac{\sigma_{III}}{V_o}\left[\frac{1+\sin\phi_e}{2\sin\phi_e}\right]=1 \tag{4}$$

where φ_c is the friction angle for compression ($\sigma_{II}=\sigma_{III}$) and φ_e is the friction angle for extension ($\sigma_{II}=\sigma_{I}$). PMC can be evaluated by performing conventional triaxial testing on a right circular cylinder, where axial stress σ_a is applied independent of radial stress σ_r so that either compression failure (axial shortening) or extension failure (axial lengthening) can be achieved. Several researchers [*Kirkpatrick*, 1957; *Roscoe et al.*, 1958; *Henkel*, 1960; *Hvorslev*, 1960; *Parry*, 1960; *Bishop*, 1966] noted that the internal friction angle for soils can be

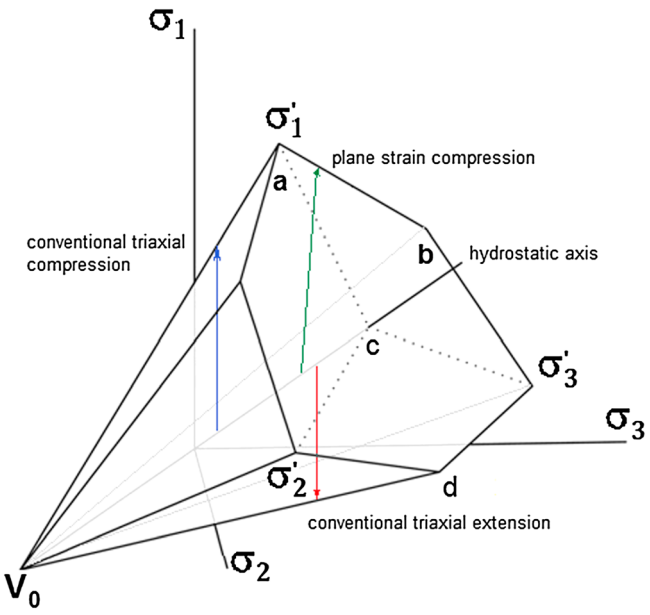

Figure 1. Linear failure surface in principal stress space with designated stress paths.

different for compression and extension, which implies an intermediate stress effect, but a failure criterion was not generalized to include a strength parameter such as S_o or V_o.

This letter provides a basis for the use of the Paul-Mohr-Coulomb criterion implementing a plane fitting approach. Conventional triaxial compression, conventional triaxial extension, and plane strain compression tests were performed on Berea sandstone. The triaxial data were plotted in principal stress space, and material parameters were determined in the context of friction angles φ_c, φ_e, and V_o, which is the vertex of a six-sided failure surface in principal stress space (Figure 1). The contribution of this work is the use of plane fitting and the development of a 12-sided failure surface with four friction angles and two different vertices.

2. Background

For isotropic rock, the strength properties of which are the same in all directions, the orientation of the principal stresses does not matter, and principal stresses can be designated σ_1, σ_2, and σ_3 with no regard to order. Therefore, the representation of equation (1) or (3) in σ_1, σ_2, and σ_3 space gives an irregular hexagonal pyramid because of the six planes for the six orderings of the principal stresses (Figure 1). Certain features are readily identified: (a) the intersection of the failure surface with the hydrostatic axis ($\sigma_1 = \sigma_2 = \sigma_3$) gives V_o, and this point is not measured but it is a basic geometric feature of any pyramidal failure surface; (b) the plane normal to the hydrostatic axis is called the π plane and the projections of the coordinate axes are labeled σ'_1, σ'_2, and σ'_3; and (c) various stress paths can be described, such as conventional triaxial compression and extension. With multiaxial testing, e.g., plane strain compression, the failure surface can be enhanced, and a 12-sided pyramid can be constructed from two sets of equation (4) with five (four friction angles and the same V_o) or six (four friction angles and two values of V_o) material parameters [*Meyer and Labuz*, 2013].

3. Experimental Methods

A homogeneous block of Berea sandstone was selected for testing. The sandstone is fine grained (0.12–0.25 mm) and composed mainly of subrounded to rounded quartz grains with density $\rho = 2060\,\mathrm{kg/m^3}$. A single block, 305 × 305 × 245 mm (x, y, z axes), was used to fabricate all specimens. Ultrasonic velocity measurements showed that the rock has a low level of anisotropy: P wave and S wave velocities (c_p [km/s], c_s [km/s]) in x, y, and z directions were (2.28, 1.41), (2.13, 1.36), and (2.11, 1.35), a 7% directional variation. Also, uniaxial compressive strength (UCS or C_o) tests were performed on six cylindrical specimens (height = 105 mm, diameter = 50 mm) and loaded at an axial displacement rate of 5×10^{-4} mm/s. The UCS measured in the direction perpendicular to the bedding planes was 41–43 MPa and 40–41 MPa parallel to the beds. Although slightly anisotropic in elasticity and UCS, any directional dependency on strength was not considered.

Conventional triaxial testing involves two principal stresses developed by fluid pressure, and the stress state can be described by $\sigma_1 = \sigma_a$, $\sigma_2 = \sigma_3 = \sigma_r$. Triaxial compression loading was performed with $\sigma_a = \sigma_\mathrm{I}$, σ_r = constant, and $\Delta\sigma_a > 0$ until failure; extension unloading was performed with $\sigma_a = \sigma_\mathrm{III}$, σ_r = constant, and $\Delta\sigma_a < 0$ until failure. Ten triaxial tests were conducted on dry Berea sandstone specimens with the axial stress applied perpendicular to the beds at an axial displacement rate of $\pm 5 \times 10^{-4}$ mm/s, where the plus sign was

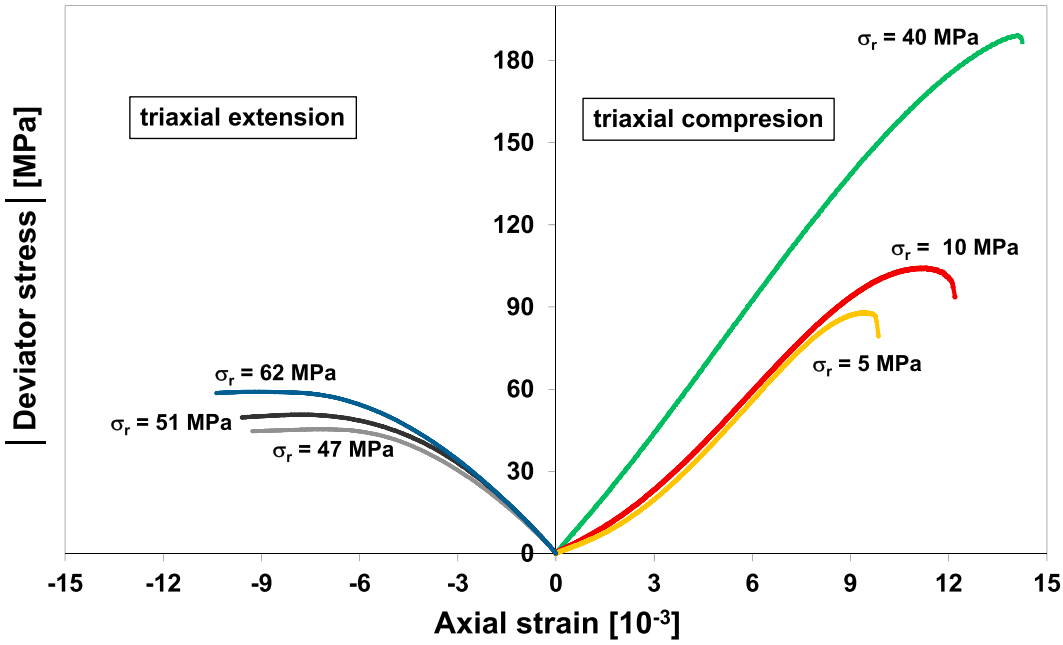

Figure 2. Mechanical behavior of Berea sandstone in conventional triaxial testing, where two principal stresses ($\sigma_I \geq \sigma_{II} \geq \sigma_{III}$) are equal to the radial stress σ_r. The right side shows the response under triaxial compression, where $\sigma_{II} = \sigma_{III} = \sigma_r$, and the left side shows the response under triaxial extension, where $\sigma_{II} = \sigma_I = \sigma_r$.

associated with compression loading and the minus sign with extension unloading. Of the 10 triaxial tests, 5 were performed in compression and 5 in extension. Additionally, a plane strain apparatus [*Makhnenko and Labuz*, 2014] was used to investigate failure for the case of $\sigma_I \neq \sigma_{II} \neq \sigma_{III}$. The plane strain condition was achieved through passive restraint by securing the specimen in a thick-walled steel cylinder. Thus, plane strain is an approximation, but the measured deformation of the steel cylinder using foil strain gages allows a calculation of the intermediate principal stress within ±0.2 MPa. The minor principal stress σ_{III} was preserved constant, and the major principal stress σ_I was increased until failure. Five plane strain compression experiments were conducted: two tests were performed at $\sigma_{III} = 0$ and the other three tests at $\sigma_{III} = 5$, 6, and 8 MPa. Stearic acid was used to reduce frictional constraint and promote homogeneous deformation for all specimens [*Labuz and Bridell*, 1993].

Table 1. Principal Stresses at Failure for Plane Strain Compression (BXC) and Conventional Triaxial Compression (TXCO) and Extension (TXEX) Experiments

Test Name	σ_I (MPa)	σ_{II} (MPa)	σ_{III} (MPa)
BXC0-1	58.7	24.2	0.0
BXC0-2	45.3	15.3	0.0
BXC5-3	82.1	33.1	5.0
BXC6-4	95.6	40.9	6.0
BXC8-5	96.9	42.3	8.0
TXCO-1	93.3	5.0	5.0
TXCO-2	114.0	10.0	10.0
TXCO-3	138.6	20.0	20.0
TXCO-4	197.2	30.0	30.0
TXCO-5	229.3	40.0	40.0
TXEX-6	62.0	62.0	2.24
TXEX-7	60.0	60.0	1.79
TXEX-8	57.0	57.0	1.56
TXEX-9	51.0	51.0	2.10
TXEX-10	47.0	47.0	1.48

4. Results

Mechanical response, given by the absolute value of the deviatoric stress ($\sigma_a - \sigma_r$) versus axial strain, from triaxial compression and extension tests are presented in Figure 2 and the results are contained in Table 1. For the axisymmetric stress states, the data are conveniently represented in the *P-q* diagram of Figure 3a, where P = mean stress = $(\sigma_a + 2\sigma_r)/3$ and q = deviatoric stress = $\sqrt{3J_2} = (\sigma_a - \sigma_r)$, where J_2 is the second invariant of the deviator stress $S_{ij} = \sigma_{ij} - P\delta_{ij}$; compression tests give $q > 0$ and extension $q < 0$. The *P-q* plane represents the section $V_o acd$ of the pyramid in Figure 1. In general,

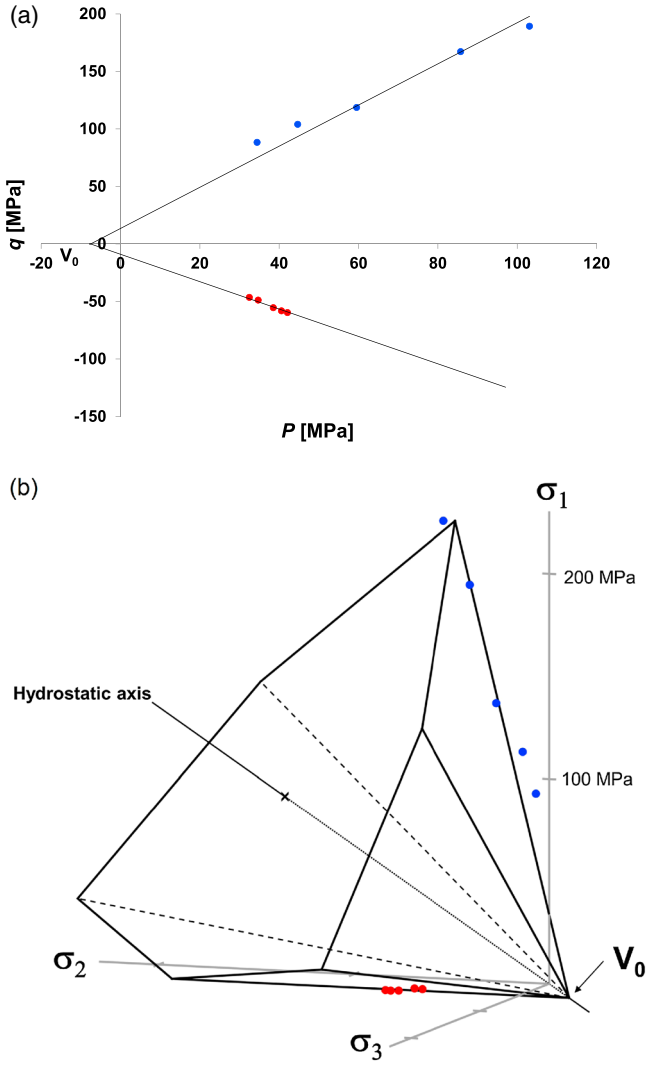

Figure 3. Failure data for dry Berea sandstone; red and blue circles represent conventional triaxial extension and compression data. (a) *q*-*P* plane. (b) Principal stress space.

the best fit lines to the compression and extension data in the *P*-*q* plane will not intersect at the same point along the *P* axis and a constraint in the fitting process must be added. Different friction angles in compression and extension were observed: $\varphi_c = 43.6°$, $\varphi_e = 47.9°$, and $V_o = 7.5$ MPa; the triaxial data and six-sided pyramid are depicted in principal stress space in Figure 3b. The friction angle in extension being larger than the one measured in compression is a sufficient but not necessary condition of the intermediate stress effect; i.e., the friction angles can be equal but failure at other stress states may depend on σ_{II}. Multiaxial testing is needed to discern the influence.

It is natural to consider a plane fitting approach to determine the material parameters, and the assumption of isotropy allows the extension data to be moved to the plane of the failure surface containing the compression data. Consider the plane $V_o ab$ (Figure 1) that contains $\sigma_1 = \sigma_I$ and $\sigma_2 = \sigma_3 = \sigma_{III}$. The extension data were translated to this plane simply by switching σ_1 and σ_2 so that $\sigma_1 = \sigma_3 = \sigma_I$ and $\sigma_2 = \sigma_{III}$. A plane describing the failure surface could then be fitted through a least squares approach that was scaled by the range of the data sets.

The least squares fit involves finding the minimum of the sum of squared orthogonal "distances" in terms of stress magnitude, between the points and the plane. With the equation of the plane written as $A\sigma_1 + B\sigma_2 + C\sigma_3 = 1$, the sum of squared distances is:

$$\sum \delta_i^2 = \frac{1}{A^2 + B^2 + C^2} \sum \left(A\sigma_{1,i} + B\sigma_{2,i} + C\sigma_{3,i} - 1\right)^2 \tag{5}$$

where δ_i is the orthogonal stress magnitude between point $i = (\sigma_{1,i}, \sigma_{2,i}, \sigma_{3,i})$ and the plane. A normalization technique with a scaling factor α was used because the compression data spanned a much larger range than the extension data. The normalized plane fitting equation is:

$$\frac{\sum \delta_{j,c}^2}{r_c^2} + \frac{\sum \delta_{k,e}^2}{\alpha r_e^2} = \text{minimum} \tag{6}$$

where $r_{c,e}$ is the maximum range in principal stress space between data points from compression, extension tests ($r_c = 144.7$ MPa, $r_e = 19.8$ MPa). Partial derivatives with respect to *A*–*C* were computed, set equal to zero, and the system of equations was solved. V_o was determined by finding the point where the plane intersects the hydrostatic axis ($\sigma_1 = \sigma_2 = \sigma_3$). The other five sides of the six-sided pyramidal failure surface were formed by exchanging the values of *A*–*C*. The results of the procedure in terms of V_o, φ_c, and φ_e are presented in Table 2, and the hexagonal pyramid is shown in Figure 3b. With $\alpha = 1.5$, determined by trial and error, both

Table 2. Line and Plane Fitting Results for Compression and Extension Data, and Plane Fitting Results for Compression, Extension, and Plane Strain Data

Line Fitting With Constraint *P-q* Plane	One Plane, Normalized Least Squares, $\alpha = 1.5$	One Plane, Normalized Least Squares, $\alpha = 1.0$	Two Planes, Normalized Least Squares, $\alpha = 1.5$	Two Planes, Normalized Least Squares, $\alpha = 1.0$
		Berea Sandstone		
$V_o = 7.5$ MPa $\phi_c = 43.6°$ $\phi_e = 47.9°$ $R_c^2 = 0.964$ $R_e^2 = 0.951$	$V_o = 7.5$ MPa $\phi_c = 43.6°$ $\phi_e = 47.9°$	$V_o = 3.86$ MPa $\phi_c = 45.8°$ $\phi_e = 55.7°$	PL 1: $V_o^{(1)} = 12.4$ MPa $\phi_c^{(1)} = 41.4°$ $\phi_e^{(1)} = 48.2°$ PL 2: $V_o^{(2)} = 5.7$ MPa $\phi_c^{(2)} = 52.2°$ $\phi_e^{(2)} = 51.4°$	PL 1: $V_o^{(1)} = 12.4$ MPa $\phi_c^{(1)} = 41.4°$ $\phi_e^{(1)} = 48.2°$ PL 2: $V_o^{(2)} = 3.8$ MPa $\phi_c^{(2)} = 54.6°$ $\phi_e^{(2)} = 55.8°$
		Indiana Limestone		
$V_o = 18.5$ MPa $\phi_c = 32.1°$ $\phi_e = 35.4°$ $R_c^2 = 0.926$ $R_e^2 = 0.926$	$V_o = 24.7$ MPa $\phi_c = 29.6°$ $\phi_e = 30.9°$	$V_o = 17.8$ MPa $\phi_c = 32.5°$ $\phi_e = 36.0°$	PL 1: $V_o^{(1)} = 22.5$ MPa $\phi_c^{(1)} = 31.0°$ $\phi_e^{(1)} = 37.6°$ PL 2: $V_o^{(2)} = 7.4$ MPa $\phi_c^{(2)} = 45.5°$ $\phi_e^{(2)} = 48.7°$	PL 1: $V_o^{(1)} = 22.5$ MPa $\phi_c^{(1)} = 31.0°$ $\phi_e^{(1)} = 37.6°$ PL 2: $V_o^{(2)} = 7.0$ MPa $\phi_c^{(2)} = 46.0°$ $\phi_e^{(2)} = 49.6°$

line fitting with a constraint and plane fitting give the same results; with $\alpha = 1.0$, the friction angles are larger than the values from the line fitting, which demonstrates the value of the scaling factor.

To provide a better fit to data from multiaxial testing, e.g., the plane strain experiments ($r_b = 58.8$ MPa), PMC was extended to form a 12-sided pyramid (Figure 4a), constructed with best fit planes using $\alpha = 1.5$ for the extension data. Similar to the method presented for the six-sided pyramid, equations of two independent planes were determined. One plane (PL 1) contains the fitted data for compression and plane strain experiments, and the other plane (PL 2) contains the fitted data for extension and plane strain experiments. Due to isotropy, there are six ways to orient these two planes, which means that a 12-sided pyramidal failure surface can be constructed. The two fitted planes are each associated with three material parameters ($V_o^{(i)}$, $\varphi_c^{(i)}$, and $\varphi_e^{(i)}$), $i = 1, 2$ to give a total of six (Table 2). As shown in the π plane described by $P = constant$ at four different values of P corresponding to the plane strain data (Figure 4b), the broken portions of the planes are not realized at every π plane section, in that the failure response is reached along a particular stress path, e.g., at $S^{(2)}$, before the stress state associated with the other portion of the plane, e.g., at $S^{(1)}$. The triaxial data are not shown in Figure 4b because these tests were associated with different values of P.

A similar construction was applied to data for Indiana limestone [*Makhnenko and Labuz*, 2014], and the results are contained in Table 2. A scaling factor $\alpha = 1.0$ provided a good match with the line fitting for the data range from compression ($r_c = 72.7$ MPa) and extension ($r_e = 17.0$ MPa) tests to form the six-sided pyramid, and $\alpha = 1.5$ is included for comparison. Different friction angles in compression and extension were observed: $\varphi_c = 32.5°$, $\varphi_e = 36.0°$, and $V_o = 17.8$ MPa. The predictions of failure when comparing PMC with two friction angles to MC with one friction angle depend on the material parameters and the stress state. For Indiana limestone and Berea sandstone at $\sigma_{III} = 10$ MPa, there is a 16% and 20% difference in σ_I for triaxial extension, and in plane strain, only a 4–5% difference, which is within the strength heterogeneity of the rock. To better fit the plane strain data ($r_b = 59.3$ MPa), a 12-sided failure surface was constructed, and two values of V_o were found, along with the four friction angles. It should be noted that the 12-sided pyramid is consistent with other true-triaxial results [e.g., *Haimson and Rudnicki*, 2010] that show a "peak" in a $\sigma_I - \sigma_{II}$ plot of failure data for fixed values of σ_{III}; this is not a feature of the six-sided failure surface.

It is interesting to evaluate the consequences of two values of V_o, which is allowed within the PMC model, and the plane fitting for both Berea sandstone and Indiana limestone displays this feature, although the discussion will be limited to the results for Berea sandstone: (a) depending on the mean stress, the shape in the π plane changes, as indicated by the four sections in Figure 4b; (b) at a low mean stress of $P = 19.4$ MPa, the 12-sided pyramid switches to 6 sided at section D_1, D_2, D_3, and PL 2 controls failure, as shown in

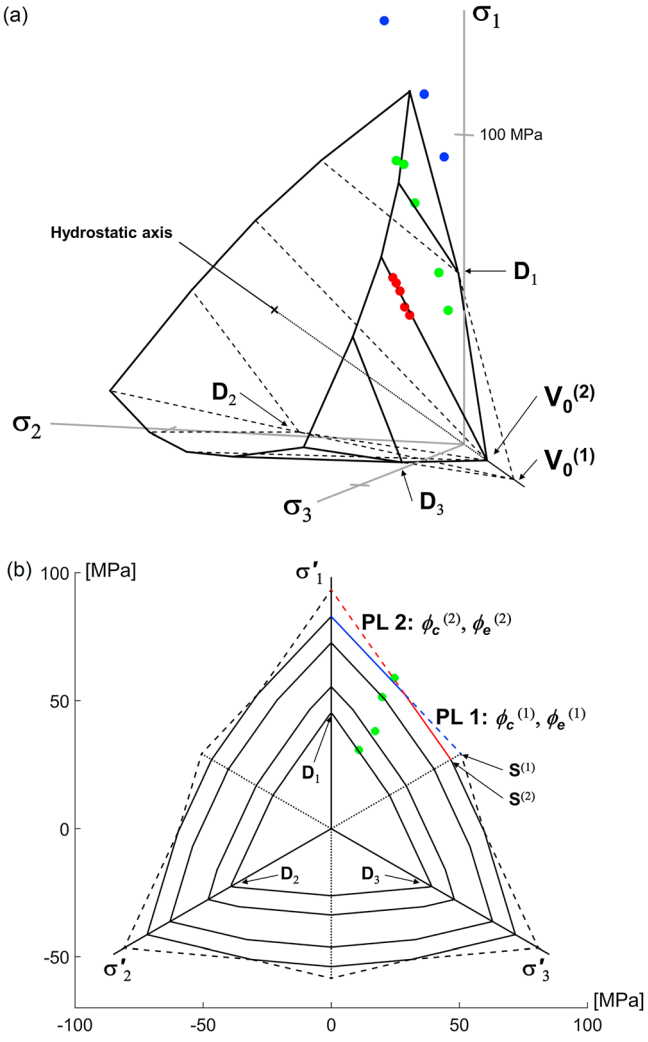

Figure 4. Paul-Mohr-Coulomb (PMC) failure surface featuring the 12-sided pyramid constructed from best fit planes and two values of V_o; from section D_1, D_2, D_3, to $V_o^{(2)}$, the failure surface switches to a six-sided pyramid. (a) PMC failure surface in principal stress space with data from conventional triaxial extension (red circles), compression (blue circles), and plane strain compression (green circles) tests. (b) The π plane representation of the failure surface at four values of mean stress P; three values of P show the irregular dodecagon, while the lowest P plotted displays the irregular hexagon.

Figures 4a and 4b; (c) at a high mean stress of $P = 169.5$ MPa (not shown), the failure surface switches back to six-sided and PL 1 controls. Thus, with two values of V_o, two, six-sided pyramids are positioned to form a 12-sided pyramid over some region ($19.9 < P < 169.5$ MPa for Berea sandstone); outside this region, at both low and high P, a six-sided pyramid—the "inner" one—is the failure surface. The values of P where the switch from 6 to 12 to 6 sides occur are determined by the six material parameters.

It should be emphasized that PMC applies for response in the brittle regime displaying shear-type failure, and it must be modified when the mean stress is large (using a "cap" model), or when one or more principal stresses are tensile (using tension cutoffs). The maximum applied mean stresses for Berea sandstone and Indiana limestone were 110 MPa and 70 MPa, respectively, and the transition to the "cap" was not observed, so the criterion is applicable at least up to these values. Moreover, at low mean stress but $P > 0$, such as in the uniaxial compression test, the failure mode typically is axial splitting and a distinct failure plane is not present. In some sense PMC is detecting a change in behavior at low mean stress, and for Berea sandstone, PL 2 gives $\varphi_e^{(2)} < \varphi_c^{(2)}$ with $\alpha = 1.5$ but $\varphi_e^{(2)} > \varphi_c^{(2)}$ with $\alpha = 1.0$ (Table 2). Nonetheless, PMC is a convenient approximation to the actual nonlinear response of rock, and features such as two values of V_o should be viewed in the context of the model.

5. Summary

The failure of Berea sandstone and Indiana limestone was considered in the framework of the Paul-Mohr-Coulomb (PMC) criterion, which includes the intermediate principal stress. Conventional triaxial compression and extension tests were conducted and used to determine the theoretical uniform triaxial (all-around equal) tensile strength V_o and friction angles in compression and extension. Assuming isotropy of the rock, a six-sided pyramidal failure surface was constructed in principal stress space using both linear and plane data fitting. PMC highlights a sufficient but not necessary condition of the intermediate stress effect: the friction angle measured in conventional triaxial extension tests was larger than the one measured from compression tests. Furthermore, the six-sided failure surface can be modified to include data from multiaxial (e.g., plane strain) compression. For that purpose, PMC was extended to form a 12-sided pyramid with six material parameters (four friction angles and two values of V_o), constructed with best fit planes and the assumption of isotropy. Thus, to predict the response of rock with three principal stresses in the brittle regime, PMC provides a simple mathematical description with recognizable material parameters.

Acknowledgments
The data are available through the University of Minnesota (UMN) Conservancy by contacting the corresponding author. Partial support was provided by the DOE grant DE-FE0002020 and the UMN Undergraduate Research Opportunities Program (UROP).

The Editor thanks two anonymous reviewers for their assistance in evaluating this paper.

References

Bishop, A. W. (1966), The strength of soils as engineering materials, *Geotechnique*, *16*(2), 91–128.
Cornet, F. (2015), *Elements of Crustal Geomechanics*, 490 pp., Cambridge Univ. Press, Cambridge, U. K.
Di Maggio, F. L., and I. S. Sandler (1971), Material model for granular soils, *J. Eng. Mech. Div.*, *97*, 935–950.
Haimson, B., and J. W. Rudnicki (2010), The effect of the intermediate principal stress on fault formation and fault angle in siltstone, *J. Struct. Geol.*, *32*, 1701–1711.
Haythornthwaite, R. M. (1962), Range of yield condition in ideal plasticity, *Trans. ASCE*, *127*(Part I), 1252–1267.
Henkel, D. J. (1960), The shear strength of saturated remoulded clays, in *Proceedings of Research Conference on Shear Strength of Cohesive Soils*, pp. 533–554, ASCE, Univ. of Colo., Boulder, Colo.
Hvorslev, M. J. (1960), Physical components of the shear strength of saturated clays, in *Proceedings of Research Conference on Shear Strength of Cohesive Soils*, pp. 169–273, ASCE, Univ. of Colo., Boulder, Colo.
Ingraham, M. D., K. A. Issen, and D. J. Holcomb (2013), Response of Castlegate sandstone to true triaxial states of stress, *J. Geophys. Res. Solid Earth*, *118*, 536–552, doi:10.1002/jgrb.50084.
Kirkpatrick, W. M. (1957), Condition of failure for sands, in *Proceedings of 4th International Conference on Soil Mechanics*, vol. 1, pp. 172–178, Butterworths, London.
Labuz, J. F., and J. M. Bridell (1993), Reducing frictional constraint in compression testing through lubrication, *Int. J. Rock Mech. Min. Sci. Geomech. Abstr.*, *30*, 451–455.
Makhnenko, R., and J. Labuz (2014), Plane strain testing with passive restraint, *Rock Mech. Rock Eng.*, *47*(6), 2021–2029, doi:10.1007/s00603-013-0508-2.
Meyer, J. P., and J. F. Labuz (2013), Linear failure criteria with three principal stresses, *Int. J. Rock Mech. Min. Sci.*, *60*, 180–187, doi:10.1016/j.ijrmms.2012.12.040.
Mogi, K. (2007), *Experimental Rock Mechanics*, 361 pp., Taylor & Francis Group, London.
Parry, R. H. G. (1960), Triaxial compression and extension tests on remoulded saturated clay, *Geotechnique*, *10*, 166–180.
Paterson, M. S., and T.-f. Wong (2005), *Experimental Rock Deformation—The Brittle Field*, 2nd ed., 347 pp., Springer, Berlin.
Paul, B. (1961), A modification of the Coulomb-Mohr theory of fracture, *J. Appl. Mech.*, *28*, 259–268.
Paul, B. (1968), Generalized pyramidal fracture and yield criteria, *Int. J. Solids Struct.*, *4*, 175–196.
Roscoe, K. H., A. N. Schofield, and C. P. Wroth (1958), On the yielding of soils, *Geotechnique*, *8*(1), 22–53.